

Observation of broad p-wave Feshbach resonances in ultracold ^{85}Rb - ^{87}Rb mixtures

Shen Dong,¹ Yue Cui,¹ Chuyang Shen,¹ Yewei Wu,^{1,*} Meng Khoon Tey,^{1,2,†} Li You,^{1,2,‡} and Bo Gao^{3,§}

¹*State Key Laboratory of Low Dimensional Quantum Physics,
Department of Physics, Tsinghua University, Beijing 100084, China*
²*Collaborative Innovation Center of Quantum Matter, Beijing, China*

³*Department of Physics and Astronomy, University of Toledo, Mailstop 111, Toledo, Ohio 43606, USA*

(Dated: January 27, 2023)

We observe new Feshbach resonances in ultracold mixtures of ^{85}Rb and ^{87}Rb atoms in the $^{85}\text{Rb}|2, +2\rangle + ^{87}\text{Rb}|1, +1\rangle$ and $^{85}\text{Rb}|2, -2\rangle + ^{87}\text{Rb}|1, -1\rangle$ scattering channels. The positions and properties of the resonances are predicted and characterized using the semi-analytic multichannel quantum-defect theory by Gao. Of particular interest, a number of broad entrance-channel dominated p-wave resonances are identified, implicating exciting opportunities for studying a variety of p-wave interaction dominated physics.

PACS numbers: 34.50.Cx, 67.85.-d, 67.60.Bc, 34.10.+x

I. INTRODUCTION

Feshbach resonance (FR) is a powerful toolbox in the field of ultracold atoms [1]. It occurs when the energy of two scattering atoms becomes quasi-degenerate with their molecular state in a different spin configuration. Experimentally, one can tune two atoms into a FR by changing magnetic field taking advantage of the differential magnetic dipole moment between the atomic state and the molecular state. Magnetically-induced FRs have found tremendous applications. They have been used, for instance, to control scattering and loss properties of cold atomic gases [1–4], to study universal few-body physics such as Efimov states [1, 5–7], to create Feshbach or ro-vibrational ground state molecules [8–11], and to study BEC-BCS crossover and Fermi gases in the unitarity limit [12–18].

Many of the aforementioned applications make use of “broad” s-wave FRs whose properties are dominated by the entrance (open) channel. These resonances acquire the universal behavior demonstrated by a single-channel resonance and therefore are useful for studying universal properties in few-body and many-body atomic systems. There exist a number of “broad” s-wave FRs in ultracold alkali-metal systems, for both intraspecies [19–23] and interspecies [24–30] mixtures. However, it is not clear if “broad” FRs also exist for the higher partial waves. This is because the criterion for distinguishing “broad” and “narrow” non-s-wave FRs was not established firmly until the multichannel quantum-defect theory (MQDT) is extended to neutral atom collision with van der Waals interactions [31, 32]. This theory enables a uniform approach to treat FRs in higher partial waves as in the s-wave, it can therefore provide a rigorous definition of

“broad” FRs for all partial waves [32]. The first application of this model to the mixture of ^6Li and ^{40}K [33] found all resonances, both s-wave and higher partial waves, to be closed-channel dominated and therefore are all “narrow” resonances.

In this paper, we apply the semi-analytic MQDT [32, 33] to predict and characterize FRs in different spin and partial-wave channels of a ^{85}Rb - ^{87}Rb mixture. We find that this mixture exhibits a rich spectrum of “broad” s-wave and p-wave FRs. The predicted FRs are observed and verified experimentally. In particular, a very broad entrance-channel-dominated p-wave resonance we discovered in the lowest energy channel of the system suggests exciting opportunities for investigating universal few-body and many-body behaviors with strong coupling in nonzero partial waves [34–39], including p-wave bosonic superfluid mixture, three-body recombination decay, and formation of p-wave heteronuclear molecules.

II. “BROAD” OR “NARROW”

Besides theoretical curiosity, a main motivation for distinguishing whether a FR is intrinsically “broad” or “narrow” is to determine its usefulness for studying universal properties of strongly interacting few-body and many-body atomic systems at low temperatures. For cold neutral atoms in the ground states, such universal properties arise from the common long-range $1/R^6$ type (R being the interatomic separation) attractive potential between the atoms, and the fact that low-temperature near-threshold scattering wave functions of these systems are predominantly shaped by the long-range potential [1, 40]. Since collision of real atoms is intrinsically a multichannel process, systems near a FR (which provides the required strong interactions) might or might not exhibit universal behaviors expected for single-channel collisions. This explains the interest in identifying “broad” FRs.

A “broad” FR is technically defined as one that shows universal characteristics of a single-channel collision over a large fraction of its resonance width, where the over-

* Present address: JILA, University of Colorado at Boulder, Boulder, CO 80309.

† mengkhoon.tey@mail.tsinghua.edu.cn

‡ lyou@mail.tsinghua.edu.cn

§ bo.gao@utoledo.edu

all wave function of the colliding atoms is dominated by that from the entrance channel over that from the quasi-degenerate closed channel. A nice and detailed discussion about the characteristics of “broad” s-wave FRs can be found in Ref. [1]. Here, we extend the discussion to include higher partial waves from the perspective of the semi-analytic MQDT.

Considering a simple two-atom scattering with only one channel, the physics of the system near the threshold energy is almost independent of the details of the short-range interactions. It can be fully determined by the long-range potential and a quantum-defect parameter which takes in the effect of the short-range interactions. This quantum defect depends weakly on the energy and the partial wave quantum number l of the system under study. For quantum-defect theory (QDT) based on the analytic solutions to the Schrödinger equation with a $-1/R^6$ potential [31, 32, 41], the near-threshold physics of the system can be studied most efficiently by replacing the real molecular potential by a pure $-\frac{C_6}{R^6} + \frac{\hbar^2}{2\mu} \frac{l(l+1)}{R^2}$ potential which is cut off by a sharp infinite repulsive wall at R_W at sufficiently small R (see Fig. 1 for illustration). Here, the $\frac{\hbar^2}{2\mu} \frac{l(l+1)}{R^2}$ term represents the centrifugal barrier of the l -th partial wave and C_6 is the actual van der Waals interaction coefficient for the system. The infinite wall sets the boundary conditions and defines the relative phase between the incoming and outgoing wave functions at small R , effectively replacing the short-range potential. In QDT, its effect is represented by the short-range K matrix (K^c) or its equivalent - the quantum defect μ^c [42–45].

For a real atomic system with many scattering channels, the problem can be reduced to an effective single-channel problem using an effective short-range K_{eff}^c matrix which takes into account the influence of all channels [31, 32, 46, 47]. In this scenario (MQDT), the equivalent parameter $R_W(\epsilon)$ becomes more dependent on the energy ϵ (Fig. 1) than the single-channel scenario. For a “broad” FR, the energy dependence of K_{eff}^c or $R_W(\epsilon)$ should exert insignificant influence on the properties of the system (as a function of ϵ) set by the long-range van der Waals interaction only.

III. PREDICTING AND CHARACTERIZING FESHBACH RESONANCES OF ALL PARTIAL WAVES

We use the semi-analytic MQDT [32, 33] to predict and characterize the FRs for various partial waves in the ^{85}Rb - ^{87}Rb mixture. The model we adopt for the current study leaves out the weak magnetic dipole-dipole [48, 49] and second-order electronic spin-orbit interactions [50–52], therefore it only predicts FRs due to couplings between atomic and molecular states of the same partial wave. These FRs are typically broader and thus easier to observe. To set the benchmark for future investigations, we limit ourselves to baseline MQDT results that

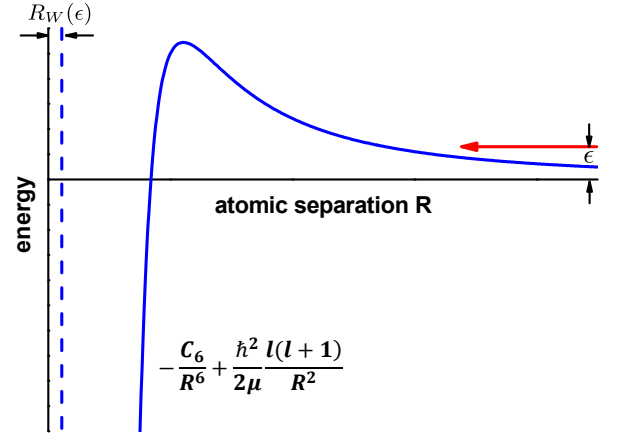


FIG. 1. (Color online) The essence of MQDT based on the analytic solutions to the Schrödinger equation with a $-1/R^6$ potential [32]. The real molecular potentials are essentially replaced by a single pure $-\frac{C_6}{R^6} + \frac{\hbar^2}{2\mu} \frac{l(l+1)}{R^2}$ potential (extended from the real long-range potential) cut off by a sharp infinite repulsive wall (dashed line) at R_W which accounts for the multichannel effect from short ranges. The effective “quantum defect” $R_W(\epsilon)$ depends sensitively on the scattering energy ϵ for a “narrow” FR.

ignore the weak energy and partial-wave dependence of the quantum defects, i.e., we adopt the approximations of $K_S^c(\epsilon, l) \approx K_S^c(\epsilon = 0, l = 0)$ and $K_T^c(\epsilon, l) \approx K_T^c(\epsilon = 0, l = 0)$ [32] for the singlet- and triplet-state short-range K-matrices, respectively. In this baseline description, all aspects of cold atomic interaction, including parameters for all magnetic FRs in all partial waves, are determined from three parameters [53, 54]: the C_6 coefficient, the singlet s-wave scattering length $a_{l=0}^S$, and the triplet s-wave scattering length $a_{l=0}^T$, apart from the well-known atomic parameters such as the atomic mass and hyperfine splitting.

The three parameters we adopt for this study are $C_6 = 4710$ a.u., $a_{l=0}^S = 11.37$ a.u. and $a_{l=0}^T = 184.0$ a.u. Both the C_6 coefficient and the singlet s-wave scattering length are taken unaltered from Ref. [55], while the triplet s-wave scattering length is adjusted from the value of 201.0 in Ref. [55] to give a better agreement with experimental s-wave FR positions in Ref. [24]. The above scattering lengths correspond to quantum defects of $\mu_S^c(\epsilon = 0, l = 0) = 0.7253$ for the singlet state and $\mu_T^c(\epsilon = 0, l = 0) = 0.2045$ for the triplet state [56]. They correspond to the short-range K matrices of $K_S^c(\epsilon, l) \approx K_S^c(\epsilon = 0, l = 0) = -0.5084$ and $K_T^c(\epsilon, l) \approx K_T^c(\epsilon = 0, l = 0) = 1.685$ [53, 56], from which the K_{eff}^c matrix in a magnetic field is constructed, and predictions and characterizations of FRs are carried out as discussed in Ref. [33].

According to the formulation and discussions in Ref. [32], around each resonance located at B_{0l} , especially an isolated resonance, the dependence of the generalized scattering length on the magnetic field can be

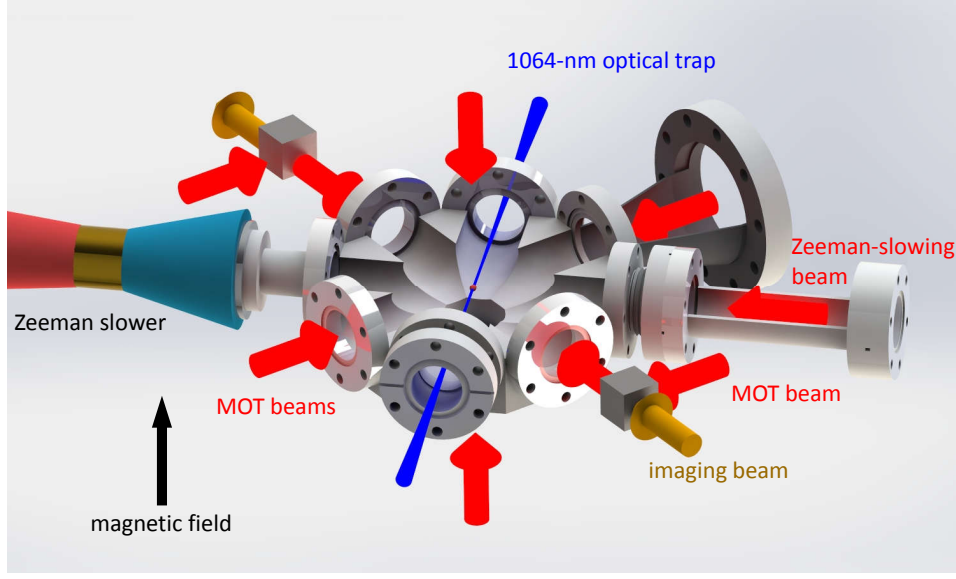


FIG. 2. (Color online) The essential elements of our experimental setup. ^{87}Rb and ^{85}Rb atoms are loaded into a magneto-optical trap from a common Zeeman slower. A 1064-nm optical dipole trap is used to confine the atoms for FR loss spectroscopy. A single bichromatic imaging beam overlapping with one of the MOT beams is used to probe the atom numbers of both species in sequence.

parameterized for all partial waves by

$$\tilde{a}_l(B) = \tilde{a}_{\text{bgl}} \left(1 - \frac{\Delta_{Bl}}{B - B_{0l}} \right), \quad (1)$$

similar to the usual form for the s-wave FRs [1]. Here, \tilde{a}_{bgl} (of dimension L^{2l+1}) is the generalized background scattering length for the l -th partial wave [57] and $|\Delta_{Bl}|$ denotes the distance from the FR position to the nearest zero- \tilde{a}_l position. These parameters, B_{0l} , \tilde{a}_{bgl} and Δ_{Bl} , together with $\delta\mu_l$ (the differential magnetic moment between the molecular state and the atomic state) [1, 32] and the C_6 coefficient, form one set of parameters that provides a complete description of atomic interaction around a magnetic FR. They constitute the most direct generalization of the s-wave description [1, 48, 58] to higher partial waves. They are easily adapted and highly efficient for treating FR at zero energy (the threshold).

A derived parameter which distinguishes a “broad” resonance ($|\zeta_{\text{res}}| \gg 1$) that follows single-channel universal behaviors from a “narrow” resonance ($|\zeta_{\text{res}}| \ll 1$) that violates such a behavior is given by [32]

$$\zeta_{\text{res}} = -\frac{1}{(2l+3)(2l-1)} \frac{\tilde{a}_{\text{bgl}}}{\bar{a}_l} \left(\frac{\delta\mu_l \Delta_{Bl}}{s_E} \right). \quad (2)$$

When $l = 0$, the parameter ζ_{res} reduces to the s-wave dimensionless resonance strength parameter s_{res} previously introduced [1] by a factor of 3. In Eq. (2), the parameter $s_E = \hbar^2/(2\mu\beta_6^2)$ is the characteristic energy scale of the van der Waals potential, with $\beta_6 = (2\mu C_6/\hbar^2)^{1/4}$ being the characteristic length scale and μ the reduced mass. The parameter $\bar{a}_l = \bar{a}_{sl}\beta_6^{2l+1}$ is the mean scatter-

ing length for the l -th partial wave, with [32]

$$\bar{a}_{sl} = \frac{\pi^2}{2^{4l+1} [\Gamma(l/2 + 1/4)\Gamma(l + 3/2)]^2}. \quad (3)$$

IV. EXPERIMENT

Figure 2 illustrates the essential elements of our experimental setup. Both ^{87}Rb and ^{85}Rb atoms are first loaded into a magneto-optical trap (MOT) from a common Zeeman slower. The ^{87}Rb atoms are loaded for 8 s while the ^{85}Rb atoms are only loaded simultaneously during the last 1 s of the ^{87}Rb loading stage. This procedure gives about 2.5×10^9 ^{87}Rb atoms and 5×10^7 ^{85}Rb atoms following the molasses cooling stage. After optical pumping both isotopes to their low-field seeking hyperfine states, $^{85}\text{Rb}|f=2, m_f=-2\rangle$ and $^{87}\text{Rb}|1, -1\rangle$, the atoms are loaded into a magnetic quadrupole trap. Forced microwave evaporation is then performed on ^{87}Rb atoms, and ^{85}Rb atoms are sympathetically cooled by the ^{87}Rb atoms to reach a common temperature of $\sim 12 \mu\text{K}$. The mixture is then loaded into an optical dipole trap formed by a single focused horizontal 1064-nm light beam, which has a $1/e^2$ waist of $\sim 35 \mu\text{m}$ and an initial power of 2.7 W. At this stage, we typically have 3.5×10^6 ^{87}Rb atoms and 4×10^6 ^{85}Rb atoms. By reducing the light power from 2.7 W to 0.25 W in 3.2 s in two linear ramps, the mixture is further cooled down to a temperature of $\sim 2 \mu\text{K}$ and ends up with approximately 1.5×10^6 ^{87}Rb atoms and 5×10^5 ^{85}Rb atoms. At this stage, the trapping frequencies are $\approx 2\pi \times (2.5, 376, 374) \text{ Hz}$ for ^{87}Rb atoms.

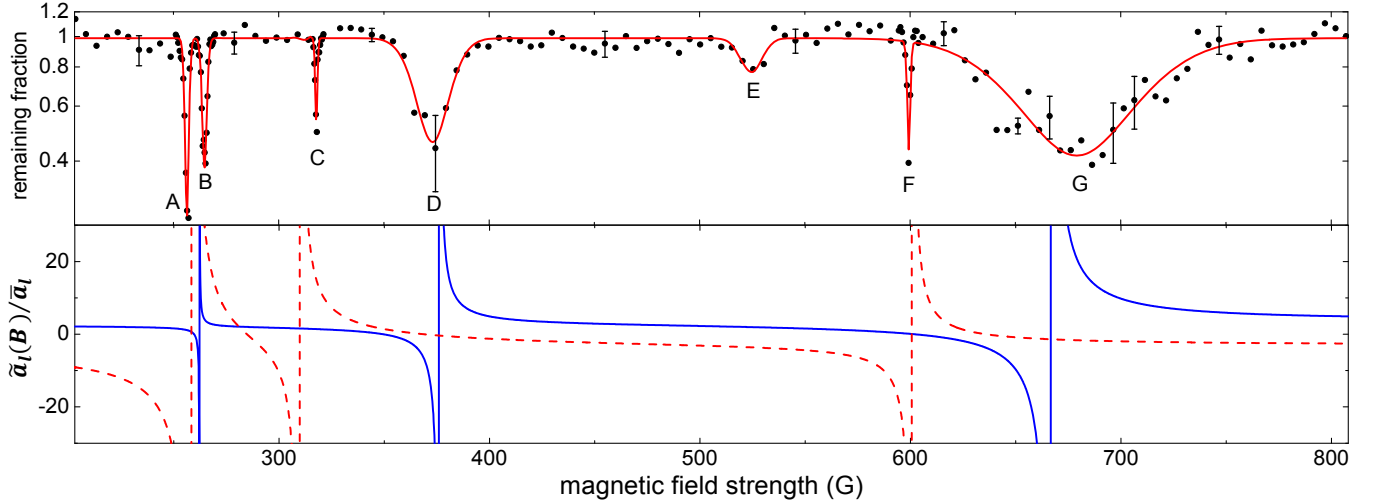


FIG. 3. (Color online) Feshbach spectrum for the $^{85}\text{Rb}|2, -2\rangle + ^{87}\text{Rb}|1, -1\rangle$ channel. Top panel: The remaining fraction of ^{85}Rb normalized to off-resonant values after 400-1000 ms interaction with ^{87}Rb at $\sim 2\mu\text{K}$ is shown as a function of magnetic field. Every data point is averaged over 5 runs. Error bars denoting typical standard deviations are shown at specific magnetic fields for illustration. We fit the data using a multi-peak Gaussian profile to get the eye-guiding line (red solid line). Bottom panel: The s-wave (blue solid line) and p-wave (red dashed line) RGSL, $\tilde{a}_l(B)/\bar{a}_l$, computed using the semi-analytic MQDT.

The remaining ^{85}Rb and ^{87}Rb atoms are then prepared into the desired spin states (scattering channels). Afterwards, we switch the magnetic field to a certain value in the range of 0-900 G and then hold the mixture for some amount of time to search for the FRs predicted by our theoretical model. The presence of FRs results in enhanced atomic scattering and three-body collision loss, and thereby shows up as loss features in the loss spectrum as a function of magnetic field. We determine the numbers of the two isotopes by absorption imaging using a CCD camera working in the fast-kinetic mode. The magnetic field strength is calibrated by measuring the Zeeman splittings of ^{87}Rb magnetic sublevels which are then compared to the Breit-Rabi results. The magnetic-field fluctuation in our system is typically about 150 mG, mainly limited by variation in the magnetization of the stainless-steel vacuum chamber in different experimental cycles.

V. RESULTS

Figure 3 shows the s-wave and p-wave FRs for the $^{85}\text{Rb}|2, -2\rangle + ^{87}\text{Rb}|1, -1\rangle$ scattering channel from 200 G to 800 G. The top panel displays the remaining ^{85}Rb fraction relative to the off-resonant values after co-existing with ^{87}Rb for typical durations from 400 ms to 1000 ms as a function of magnetic field. The bottom panel shows the predictions of the reduced generalized scattering length (RGSL), $\tilde{a}_l(B)/\bar{a}_l$, for both the s-wave (blue solid line) and p-wave (red dashed line) channels from the semi-analytic MQDT [32, 33, 57]. It is clear from the theoretical results that the features at B, D, and G correspond to the s-wave FRs, while those at A, C, and F are p-wave

FRs. The loss at E, which is present even without ^{87}Rb atoms, is due to an intraspecies FR of ^{85}Rb itself [23]. Among the resonances, A, B, D were observed previously in Ref. [24], and C was also predicted in Ref. [59].

Figure 4 displays the FRs for the $^{85}\text{Rb}|2, +2\rangle + ^{87}\text{Rb}|1, +1\rangle$ scattering channel which has not been studied before. After preparing the mixture at $\sim 2\mu\text{K}$, the ^{85}Rb and ^{87}Rb atoms are transferred to the $|2, +2\rangle$ and $|1, +1\rangle$ states, respectively, by rf adiabatic passages [60]. Our model predicts only two s-wave and two p-wave FRs for this channel from 0 to 900 G. We find three broader FRs but not the narrowest one predicted to be around 701 G. These FRs are labeled by H, I, and J in Fig. 4. The resonance at K is again due to an intraspecies FR of the ^{85}Rb atoms [23].

We identify the p-wave resonances not only by their proximity to our theoretical predictions, but also by their asymmetric line shapes and more definitely by their distinctive doublet structures [59] which can be observed when their loss-feature widths become smaller than their doublet splitting at sufficiently low temperatures. As an example, Fig. 5 shows the doublet structure of the p-wave resonance at 600 G in Fig. 3 (loss feature F) at a temperature of $\sim 400\text{ nK}$. For the broadest p-wave resonance (J in Fig. 4), we are unable to reduce the temperature of the mixture low enough to observe the doublet structure. Instead, we observe a distinctive change in the line shape when lowering the temperature of the mixture from $\sim 2\mu\text{K}$ (red diamonds) to $\sim 400\text{ nK}$ (black circles) as shown in Fig. 6. As the collision energy gets nearer to the channel's threshold, the loss feature becomes narrower and its 'threshold' edge becomes steeper. These phenomena are in agreement with the expectations for a

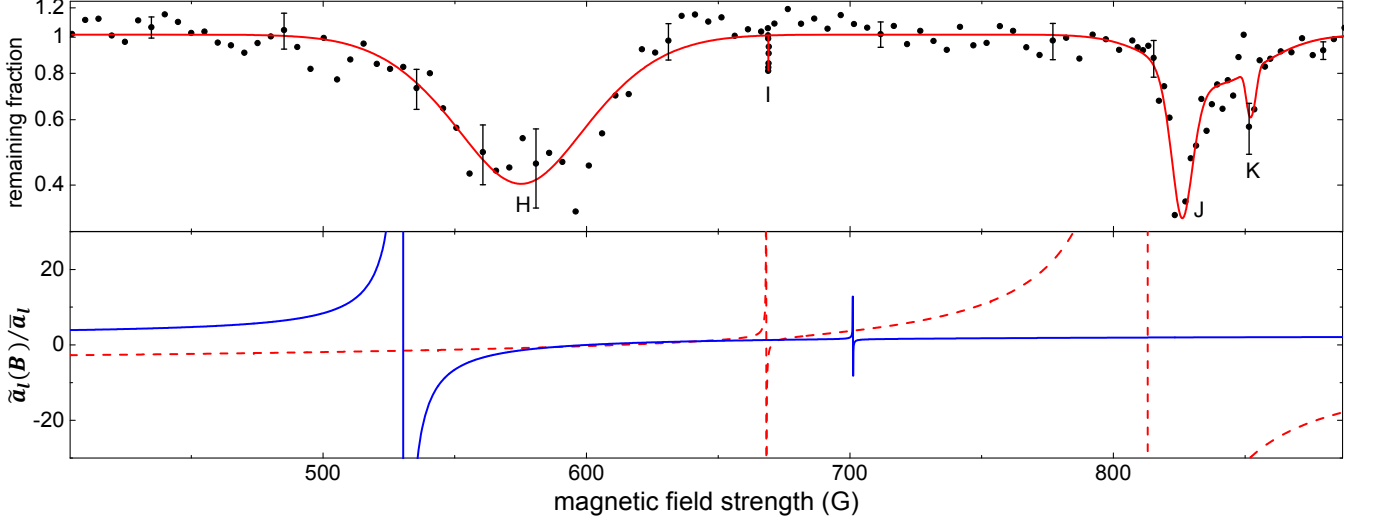


FIG. 4. (Color online) The same as in Fig. 3 but for the $^{85}\text{Rb}|2, +2\rangle + ^{87}\text{Rb}|1, +1\rangle$ channel after 600-ms interaction time.

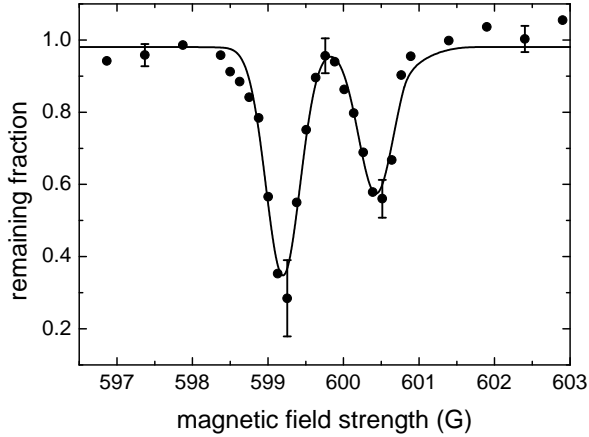


FIG. 5. A clear doublet splitting emerges in the 600-G p-wave FR in Fig. 3 (structure F) at a temperature of ~ 400 nK.

p-wave resonance [59].

The experimentally measured positions and widths of the FR loss features are tabulated in Table I, together with the theoretical predictions for the relevant resonance parameters, namely B_{0l} , \tilde{a}_{bgl} , Δ_{Bl} , $\delta\mu_l$ and ζ_{res} . The resonance centers and full-width-at-half-maximum (FWHM) of all the s-wave loss features are obtained using Gaussian fit. The positions of the p-wave resonances are determined by the intercept of the lossless baseline with the steeper edge of the p-wave loss features, while the reported widths are obtained from Gaussian fit. The reported uncertainties in the measured FR positions B_{0l}^{expt} represent the loss-feature fitting uncertainties. For fitting uncertainties smaller than 0.2 G, they are set to 0.2 G to reflect the magnetic field fluctuation in our experimental setup.

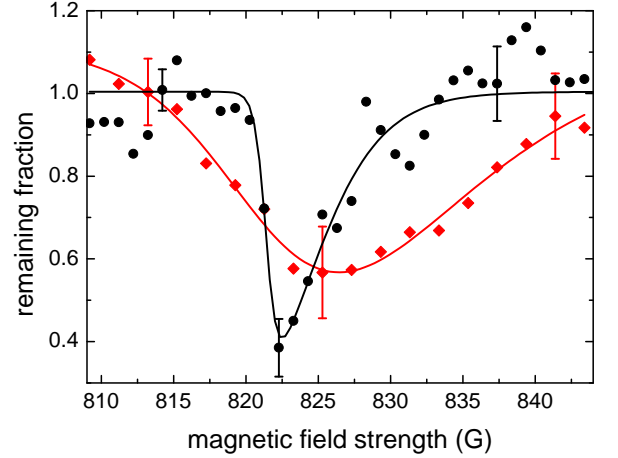


FIG. 6. (Color online) Temperature dependence of the broadest p-wave resonance in the $^{85}\text{Rb}|2, +2\rangle + ^{87}\text{Rb}|1, +1\rangle$ channel (J in Fig. 4). The loss feature narrows, and its left-edge becomes steeper as the temperature of the mixture is lowered from ~ 2 μK (red diamonds) to ~ 400 nK (black circles). The solid lines represent the fits to the data using asymmetric double sigmoid function to account for the asymmetric line shapes.

VI. DISCUSSION AND CONCLUSION

From Table I, one can observe some discrepancies between the predictions and the measured results of the FR positions. These discrepancies are generally larger than those offered by numerical coupled-channel calculations facilitated with full knowledge of the relevant molecular potentials [23, 26, 28–30, 61]. This arises from the fact that the MQDT we adopt employs the analytic solutions for an ideal long-range $1/R^6$ potential, while real molecular potentials have long-range $1/R^8$ and $1/R^{10}$ contri-

TABLE I. Theoretical and experimental parameters for the s-wave and p-wave FRs in the $^{85}\text{Rb}|2, -2\rangle + ^{87}\text{Rb}|1, -1\rangle$ and $^{85}\text{Rb}|2, +2\rangle + ^{87}\text{Rb}|1, +1\rangle$ channels in the magnetic field range of 0-900 G.

Channel	l	B_{0l}^{expt} (G)	$\delta_{Bl}^{\text{expt}}$ (G)*	B_{0l} (G)	Δ_{Bl} (G)	$\tilde{a}_{\text{bgl}}/\tilde{a}_l$	$\delta\mu_l/\mu_B$	ζ_{res}
$^{85}\text{Rb} 2, -2\rangle$	0	264.8(2)	2.3	262.2	-2.6	1.984	-1.752	2.719
$+^{87}\text{Rb} 1, -1\rangle$	0	372(1)	18	375.9	-26.4	2.458	-0.9172	17.97
	0	675(2)	73	666.7	-64.7	3.375	-1.4362	94.58
	1	257.2(2)	2.3	258.3	26.4	-10.36	-1.736	-85.95
	1	318.1(2)	0.9	309.8	59.0	-2.845	-1.817	-55.23
	1	599.3(2)	1.7	600.7	35.2	-2.847	-0.5112	-9.252
$^{85}\text{Rb} 2, +2\rangle$	0	569(1)	66	530.4	70.0	2.554	1.574	84.93
$+^{87}\text{Rb} 1, +1\rangle$	0	-	-	701.1	0.3	1.518	1.879	0.2966
	1	669.0(2)	0.04	668.3	2.0	1.998	1.873	-1.360
	1	823.3(7)	13	813.0	-142.8	-8.824	2.453	-559.0

* The parameter $\delta_{Bl}^{\text{expt}}$ represents the measured FWHM of a loss feature. It is different from Δ_{Bl} defined by Eq. (1).

butions for interatomic separations shorter than $\sim 0.3\beta_6$ (about 2.5 nm for Rb atoms). These discrepancies should be smaller if the energy- and partial-wave-dependence corrections to the quantum defects are considered. One of the advantages of the semi-analytic MQDT is that it does not require full knowledge of the molecular potentials, but only the C_6 coefficient, and the singlet and triplet s-wave scattering lengths, all of which can be determined with the measurement of a few FR positions. More importantly, the semi-analytic nature of the theory makes it more efficient and reliable for predicting FRs with non-s-wave scattering channels, particularly narrow resonances, since our approach is immune to errors that usually plague numerical calculations when handling the classically forbidden regime in the centrifugal barriers. In this regime, small numerical errors can be amplified exponentially, causing a runaway divergence.

The results from our model show that the previously observed p-wave resonance at 257.2(2) G in the $^{85}\text{Rb}|2, -2\rangle + ^{87}\text{Rb}|1, -1\rangle$ channel is a entrance-channel dominated broad resonance with $|\zeta_{\text{res}}| \approx 86$. We discover two new broad p-wave resonances at 318.1(2) G and 599.3(2) G in this channel, with $|\zeta_{\text{res}}| \approx 55$ and 9, respectively. In the $^{85}\text{Rb}|2, +2\rangle + ^{87}\text{Rb}|1, +1\rangle$ channel, an even broader p-wave resonance at 823.3(7) G with $|\zeta_{\text{res}}| \approx 559$ is discovered. The existence of so many broad high par-

tial wave FRs in ^{85}Rb and ^{87}Rb mixture is an interesting phenomenon by itself. This would be a subject for future investigations. Understanding the reasons behind this could be important for predicting new cold atomic mixtures exhibiting broad nonzero partial wave FRs.

In conclusion, we make use of the semi-analytic MQDT to predict FRs in a ^{85}Rb and ^{87}Rb mixture and discover many entrance-channel dominated p-wave FRs. Our experiment confirms the existence of these broad resonances. Of particular interest, a very broad p-wave FR is found in the lowest energy combination of the $^{85}\text{Rb}|2, +2\rangle + ^{87}\text{Rb}|1, +1\rangle$ channel with a record $|\zeta_{\text{res}}| \approx 559$. This work opens up new possibilities of investigating universal few-body and many-body behaviors in a bosonic atom mixture with strong coupling in high partial waves.

ACKNOWLEDGMENTS

This work is supported at Tsinghua by MOST (No. 2013CB922004 and No. 2014CB921403) of the National Key Basic Research Program of China, and by NSFC (No. 91121005, No. 91421305, No. 11574177, No. 11374176, No. 11328404, No. 91636213), and at Toledo by NSF (PHY-1306407 and PHY-1607256).

- [1] C. Chin, R. Grimm, P. Julienne, and E. Tiesinga, *Rev. Mod. Phys.* **82**, 1225 (2010).
- [2] S. L. Cornish, N. R. Claussen, J. L. Roberts, E. A. Cornell, and C. E. Wieman, *Phys. Rev. Lett.* **85**, 1795 (2000).
- [3] K. E. Strecker, G. B. Partridge, A. G. Truscott, and R. G. Hulet, *Nature* **417**, 150 (2002).
- [4] T. Weber, J. Herbig, M. Mark, H.-C. Nägerl, and

- R. Grimm, *Science* **299**, 232 (2003).
- [5] T. Kraemer, M. Mark, P. Waldburger, J. G. Danzl, C. Chin, B. Engeser, A. D. Lange, K. Pilch, A. Jaakkola, H.-C. Nägerl, and R. Grimm, *Nature* **440**, 315 (2006).
- [6] J. von Stecher, J. P. D’Incao, and C. H. Greene, *Nat Phys* **5**, 417 (2009).
- [7] A. N. Wenz, G. Zürn, S. Murmann, I. Brouzos, T. Lompe, and S. Jochim, *Science* **342**, 457 (2013).

- [8] C. A. Regal, C. Ticknor, J. L. Bohn, and D. S. Jin, *Nature* **424**, 47 (2003).
- [9] K.-K. Ni, S. Ospelkaus, M. H. G. de Miranda, A. Pe'er, B. Neyenhuis, J. J. Zirbel, S. Kotochigova, P. S. Julienne, D. S. Jin, and J. Ye, *Science* **322**, 231 (2008).
- [10] F. Lang, K. Winkler, C. Strauss, R. Grimm, and J. H. Denschlag, *Phys. Rev. Lett.* **101**, 133005 (2008).
- [11] J. G. Danzl, M. J. Mark, E. Haller, M. Gustavsson, R. Hart, J. Aldegunde, J. M. Hutson, and H.-C. Nägerl, *Nat Phys* **6**, 265 (2010).
- [12] J. Kinast, A. Turlapov, J. E. Thomas, Q. Chen, J. Stajic, and K. Levin, *Science* **307**, 1296 (2005).
- [13] M. Horikoshi, S. Nakajima, M. Ueda, and T. Mukaiyama, *Science* **327**, 442 (2010).
- [14] S. Nascimbène, N. Navon, K. J. Jiang, F. Chevy, and C. Salomon, *Nature* **463**, 1057 (2010).
- [15] M. J. H. Ku, A. T. Sommer, L. W. Cheuk, and M. W. Zwierlein, *Science* **335**, 563 (2012).
- [16] L. A. Sidorenkov, M. K. Tey, R. Grimm, Y.-H. Hou, L. Pitaevskii, and S. Stringari, *Nature* **498**, 78 (2013), letter.
- [17] M. K. Tey, L. A. Sidorenkov, E. R. S. Guajardo, R. Grimm, M. J. H. Ku, M. W. Zwierlein, Y.-H. Hou, L. Pitaevskii, and S. Stringari, *Phys. Rev. Lett.* **110**, 055303 (2013).
- [18] E. R. S. Guajardo, M. K. Tey, L. A. Sidorenkov, and R. Grimm, *Phys. Rev. A* **87**, 063601 (2013).
- [19] C. Chin, V. Vuletić, A. J. Kerman, and S. Chu, *Phys. Rev. Lett.* **85**, 2717 (2000).
- [20] K. Dieckmann, C. A. Stan, S. Gupta, Z. Hadzibabic, C. H. Schunck, and W. Ketterle, *Phys. Rev. Lett.* **89**, 203201 (2002).
- [21] T. Loftus, C. A. Regal, C. Ticknor, J. L. Bohn, and D. S. Jin, *Phys. Rev. Lett.* **88**, 173201 (2002).
- [22] S. Knoop, T. Schuster, R. Scelle, A. Trautmann, J. Appmeier, M. K. Oberthaler, E. Tiesinga, and E. Tiemann, *Phys. Rev. A* **83**, 042704 (2011).
- [23] C. L. Blackley, C. R. Le Sueur, J. M. Hutson, D. J. McCarron, M. P. Köppinger, H.-W. Cho, D. L. Jenkin, and S. L. Cornish, *Phys. Rev. A* **87**, 033611 (2013).
- [24] S. B. Papp and C. E. Wieman, *Phys. Rev. Lett.* **97**, 180404 (2006).
- [25] F. Ferlaino, C. D'Errico, G. Roati, M. Zaccanti, M. Inguscio, G. Modugno, and A. Simoni, *Phys. Rev. A* **73**, 040702 (2006).
- [26] E. Wille, F. M. Spiegelhalter, G. Kerner, D. Naik, A. Trenkwalder, G. Hendl, F. Schreck, R. Grimm, T. G. Tiecke, J. T. M. Walraven, S. J. J. M. F. Kokkelmans, E. Tiesinga, and P. S. Julienne, *Phys. Rev. Lett.* **100**, 053201 (2008).
- [27] B. Deh, C. Marzok, C. Zimmermann, and P. W. Courteille, *Phys. Rev. A* **77**, 010701 (2008).
- [28] M. Repp, R. Pires, J. Ulmanis, R. Heck, E. D. Kuhnle, M. Weidemüller, and E. Tiemann, *Phys. Rev. A* **87**, 010701 (2013).
- [29] H.-W. Cho, D. J. McCarron, M. P. Köppinger, D. L. Jenkin, K. L. Butler, P. S. Julienne, C. L. Blackley, C. R. Le Sueur, J. M. Hutson, and S. L. Cornish, *Phys. Rev. A* **87**, 010703 (2013).
- [30] F. Wang, D. Xiong, X. Li, D. Wang, and E. Tiemann, *Phys. Rev. A* **87**, 050702 (2013).
- [31] B. Gao, E. Tiesinga, C. J. Williams, and P. S. Julienne, *Phys. Rev. A* **72**, 042719 (2005).
- [32] B. Gao, *Phys. Rev. A* **84**, 022706 (2011).
- [33] C. Makrides and B. Gao, *Phys. Rev. A* **89**, 062718 (2014).
- [34] H. Suno, B. D. Esry, and C. H. Greene, *Phys. Rev. Lett.* **90**, 053202 (2003).
- [35] K. Günter, T. Stöferle, H. Moritz, M. Köhl, and T. Esslinger, *Phys. Rev. Lett.* **95**, 230401 (2005).
- [36] J. P. Gaebler, J. T. Stewart, J. L. Bohn, and D. S. Jin, *Phys. Rev. Lett.* **98**, 200403 (2007).
- [37] Y. Ohashi, *Phys. Rev. Lett.* **94**, 050403 (2005).
- [38] S.-G. Peng, S. Tan, and K. Jiang, *Phys. Rev. Lett.* **112**, 250401 (2014).
- [39] C. Luciuk, S. Trotzky, S. Smale, Z. Yu, S. Zhang, and J. H. Thywissen, *Nat Phys* **12**, 599 (2016), article.
- [40] B. Gao, *Phys. Rev. A* **62**, 050702 (2000).
- [41] B. Gao, *Phys. Rev. A* **58**, 1728 (1998).
- [42] U. Fano, *Phys. Rev. A* **2**, 353 (1970).
- [43] A. F. Starace, "The quantum defect theory approach," in *Photoionization and Other Probes of Many - Electron Interactions*, edited by F. J. Wuilleumier (Springer US, Boston, MA, 1976) pp. 395–406.
- [44] M. J. Seaton, *Reports on Progress in Physics* **46**, 167 (1983).
- [45] B. Gao, *Phys. Rev. A* **78**, 012702 (2008).
- [46] F. H. Mies, *The Journal of Chemical Physics* **80**, 2514 (1984).
- [47] Z. Idziaszek, A. Simoni, T. Calarco, and P. S. Julienne, *New Journal of Physics* **13**, 083005 (2011).
- [48] A. J. Moerdijk, B. J. Verhaar, and A. Axelsson, *Phys. Rev. A* **51**, 4852 (1995).
- [49] H. T. C. Stoof, J. M. V. A. Koelman, and B. J. Verhaar, *Phys. Rev. B* **38**, 4688 (1988).
- [50] F. H. Mies, C. J. Williams, P. S. Julienne, and M. Krauss, *J. Res. Natl. Inst. Stand. Technol.* **101**, 521 (1996).
- [51] S. Kotochigova, E. Tiesinga, and P. S. Julienne, *Phys. Rev. A* **63**, 012517 (2000).
- [52] P. J. Leo, C. J. Williams, and P. S. Julienne, *Phys. Rev. Lett.* **85**, 2721 (2000).
- [53] B. Gao, E. Tiesinga, C. J. Williams, and P. S. Julienne, *Phys. Rev. A* **72**, 042719 (2005).
- [54] T. M. Hanna, E. Tiesinga, and P. S. Julienne, *Phys. Rev. A* **79**, 040701 (2009).
- [55] C. Strauss, T. Takekoshi, F. Lang, K. Winkler, R. Grimm, J. Hecker Denschlag, and E. Tiemann, *Phys. Rev. A* **82**, 052514 (2010).
- [56] B. Gao, *Phys. Rev. A* **78**, 012702 (2008).
- [57] B. Gao, *Phys. Rev. A* **80**, 012702 (2009).
- [58] T. Köhler, K. Góral, and P. S. Julienne, *Rev. Mod. Phys.* **78**, 1311 (2006).
- [59] C. Ticknor, C. A. Regal, D. S. Jin, and J. L. Bohn, *Phys. Rev. A* **69**, 042712 (2004).
- [60] E. Peik, M. Ben Dahan, I. Bouchoule, Y. Castin, and C. Salomon, *Phys. Rev. A* **55**, 2989 (1997).
- [61] T. Schuster, R. Scelle, A. Trautmann, S. Knoop, M. K. Oberthaler, M. M. Haverhals, M. R. Goosen, S. J. J. M. F. Kokkelmans, and E. Tiemann, *Phys. Rev. A* **85**, 042721 (2012).